Vacuum 215 (2023) 112311

Contents lists available at ScienceDirect

Vacuum

journal homepage: www.elsevier.com/locate/vacuum

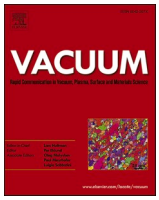

Effect of O addition on microstructure and mechanical properties of Ti-Nb alloys with various β stability

Qiang Li [a,b,*], Yan Liu [a], Huanhuan Yu [a], Masaaki Nakai [c], Mitsuo Niinomi [a,d,e,**], Kenta Yamanaka [d], Akihiko Chiba [f], Takuya Ishimoto [g], Takayoshi Nakano [e]

[a] School of Mechanical Engineering, University of Shanghai for Science and Technology, Shanghai, 200093, PR China
[b] Shanghai Engineering Research Center of High-Performance Medical Device Materials, Shanghai, 200093, PR China
[c] Department of Mechanical Engineering, Faculty of Science and Engineering, Kindai University, 3-4-1 Kowakae, Higashiosaka, Osaka, 577-8502, Japan
[d] Institute for Materials Research, Tohoku University, 2-1-1, Katahira, Aoba-ku, Sendai, 980-8577, Japan
[e] Division of Materials and Manufacturing Science, Graduate School of Engineering, Osaka University, 2-1, Yamada-Oka, Suita, Osaka, 565-0871, Japan
[f] New Industry Creation Hatchery Center, Tohoku University, 6-6-10, Aza-Aoba, Aramaki, Aoba-ku, Sendai, 980-8579, Japan
[g] Aluminium Research Center, University of Toyama, 3190, Gofuku, Toyama, 930-8555, Japan

ARTICLE INFO

Handling Editor: Prof. L.G. Hultman

Keywords:
Ti–Nb–O alloys
β phase stability
Solution strengthening
Mechanical properties

ABSTRACT

To study the effect of O on β-Ti alloys with various β phase stability, Ti–*x*Nb–0.4O (*x* = 30, 32, 34, 36, 38, 40, 42, mass%) alloys were prepared by arc melting followed by homogenization, hot rolling, and solution treatment. To ensure the O content of the alloys, melting and hot rolling were performed under an Ar atmosphere, and homogenization and solution treatment were performed under vacuum conditions. The mass fractions of O in the Ti–Nb–O alloys were finally accurately controlled in the range of 0.4–0.5%. The phase composition of the alloys was determined by analyzing the X-ray diffraction patterns, the microstructure was observed by optical microscopy, and the mechanical properties were measured by tensile tests. The ω phase and α" phase were found in the solution-treated Ti–30Nb–0.4O. Ti–30Nb–0.4O showed the lowest yield strength owing to the existence of the α" phase. O suppressed ω phase and α" phase transformations during quenching, and showed an obvious solution-strengthening effect. Because the O content of the alloys was essentially the same, the Ti–*x*Nb–0.4O alloys showed similar tensile strengths. The Young's moduli of the alloys ranged from 60 to 69 GPa, and the elongations were all higher than 15%. Particularly, Ti–36Nb–0.4O exhibited desirable mechanical properties, including a Young's modulus of 61 GPa, a tensile strength of 760 MPa, and an elongation of approximately 35%.

1. Introduction

Ti alloys are widely used in biomedical applications because of their excellent corrosion resistance and mechanical properties [1]. Commercially pure Ti (C.P.-Ti) and Ti–6Al–4V ELI are widely used in the clinical field. However, many studies have indicated that the mechanical properties of C.P.-Ti could not meet the requirements for human implantation because its abrasion resistance is low [2–4]. The release of Al and V ions from Ti–6Al–4V ELI may cause long-term health problems such as neurological diseases and Alzheimer's disease [5,6]. Additionally, the Young's moduli of C.P.-Ti and Ti–6Al–4V ELI are much higher than that of human bone, which results in a stress-shielding effect and finally causes bone resorption and implant failure. Recently, non-toxic β stabilizers such as Ta, Nb, and Mo have been added in large quantities to obtain β-type Ti alloys with improved biocompatibility [7–12]. Ti–Nb-based alloys are the most widely studied β-type Ti alloys because they generally show low Young's moduli and exhibit a shape memory effect and/or superelasticity [13–16]. Unfortunately, the β-type Ti alloys with low Young's moduli generally exhibit low strength, which limits their application [17,18]. Solution and precipitation strengthening are two feasible methods for improving the strength of β-type Ti alloys. The strength and superelasticity can be enhanced by adding Zr and Sn, which are two common alloying elements besides β stabilizing elements [19,20]. The tensile strength and fatigue performance can be increased by α phase and ω phase precipitations [21]. However, the solution-strengthening effects of Zr and Sn are limited, and the Young's

* Corresponding author. School of Mechanical Engineering, University of Shanghai for Science and Technology, Shanghai, 200093, PR China.
** Corresponding author. School of Mechanical Engineering, University of Shanghai for Science and Technology, Shanghai, 200093, PR China.
E-mail addresses: jxli@tju.edu.cn, liqiang@usst.edu.cn (Q. Li), mitsuo.niinomi.b6@tohoku.ac.jp (M. Niinomi).

https://doi.org/10.1016/j.vacuum.2023.112311
Received 10 May 2023; Received in revised form 13 June 2023; Accepted 14 June 2023
Available online 15 June 2023
0042-207X/

modulus is commonly increased by the α phase and ω phase.

As an interstitial element in Ti alloys, O shows a strong solution-strengthening effect, which increases the strength of Ti alloys [22]. Based on the first principles of density functional theory, the mutual repulsion between interstitial O atoms and substituted Nb atoms in Ti–Nb–O alloys increases the β phase stability and changes the martensite transformation behavior of Ti–Nb alloys [23,24]. The addition of O can suppress the formation of the athermal ω phase during quenching, which is beneficial for obtaining a low Young's modulus [25]. Adding O to Ti–Nb-based alloys can increase their strength and elastic strain owing to the strong interaction between the screw dislocation and the strain field generated by the O atom in the octahedral interstitial position [26–29]. In the case of O-modified Ti–Nb–Ta–Zr, the strength increases monotonically with increasing O content, whereas the elongation-to-failure first decreases and then returns to a relatively high level [30,31]. Ti–29Nb–13Ta–4.6Zr–0.7O exhibits a dislocation glide that is more homogeneous and extensive, as well as multiple slip systems in single grains and a greater frequency of cross-slip, which leads to a higher work-hardening rate and delays the occurrence of local stress concentration [30]. Unfortunately, the Young's modulus of Ti–29Nb–13Ta–4.6Zr–0.7O increases to 75 GPa, which is higher than that of Ti–29Nb–13Ta–4.6Zr. The Young's moduli of β-type Ti alloys are sensitive to the phase composition and β phase stability [32]. A low O content hardly causes a large increase in Young's modulus [33]. In Ti–(30-42)Nb alloys, the Young's modulus first increases and then decreases with an increase in the Nb content, owing to the variety of phase compositions [3,18,34]. In this study, approximately 0.4% O was added to Ti–(30-42)Nb alloys to study the effects of O on the phase, microstructure, and mechanical properties of the Ti alloys with various β stability.

2. Experiments

High-purity Ti particles (99.99%), high-purity Nb particles (99.95%), and TiO_2 powder (99.99%) were used as raw materials. The ingots with nominal components of Ti–(30, 32, 34, 36, 38, 40, 42)Nb–0.4O were prepared in a high-vacuum non-consumable arc-melting furnace with an ultimate vacuum of 5×10^{-3} Pa. Each ingot was flipped and re-melted more than five times to ensure a uniform composition. The ingots were homogenized at 1000 °C for 10 h and hot-rolled under a reduction of 80% to sheets with a thickness of 2.2 mm. The samples for the following analyses and tests were cut from the sheets by electrical discharge machining and subjected to solution treatment at 1000 °C for 1 h, followed by water quenching. Surface oxidation layers were removed by grinding with sandpaper after each heat treatment.

The O content of the alloys was determined using an inductively coupled plasma mass spectrometry. The sample for optical microstructure observation was mirror-polished with a SiO_2 suspension and etched in a 5 vol% hydrogen fluoride solution. The phase composition was determined by analyzing the X-ray diffraction (XRD) patterns obtained using a Bruker D8 Advance diffractometer with Cu–Kα radiation at a current of 40 mA, a voltage of 40 kV, and a scanning speed of 6°/min. The solution-treated specimens were mechanically polished to a thickness of approximately 50 μm using up to 2400# SiC waterproof paper, dimpled using a phosphor bronzer ring, ion-milled to a thin foil, and finally observed using JEOL JEM-2000EXII transmission electron microscopy (TEM) at a voltage of 200 kV. The Young's modulus was measured by the free-resonance method using a rectangular sample with dimensions of 40 mm × 10 mm × 1.4 mm. The transverse bending vibration of the sample was generated using an excitation signal from an excitation sensor. The resonant frequency of the sample was measured using a pickup sensor. The dynamic Young's modulus was calculated using the following equation [35]:

$$E = 0.9694(mL^3f_r^2)/(wd^3),$$

where m, L, w, and d were the weight, length, width, and thickness of the specimen, respectively, and f_r was the intrinsic resonance vibration frequency. The sample (12 mm × 3 mm × 1.4 mm) was subjected to tensile testing at room temperature (~20 °C) using an Instron-type testing machine with an applied strain gauge. The crosshead speed was 0.5 mm/min. The deformed microstructures were further analyzed using electron backscattered diffraction (EBSD).

3. Results and discussion

3.1. Chemical compositions

According to the view that the O content of Ti alloys was generally 0.1–0.2% without specific addition [34], 0.3% O was added to the alloys in the form of TiO_2 to obtain a final O content of 0.4–0.5%. The ingots were prepared in a high-vacuum furnace, homogenization and solution treatment were carried out under vacuum conditions, hot rolling was carried out under an Ar atmosphere, and finally, the O content of the alloys matched the expected values, as shown in Table 1. These results suggest that the vacuum conditions of the devices and preparation processes satisfy the requirements for preparing Ti alloys with a controllable O content.

3.2. Phases and microstructures

The XRD patterns of the Ti–xNb–0.4O alloys after solution treatment are shown in Fig. 1a. A weak diffraction peak corresponding to the α" phase was found in Ti–(30, 32, 34)Nb–0.4O alloys. The α" phase peak disappeared in Ti–(36, 38, 40, 42)Nb–0.4O alloys, which showed only β phase diffraction peaks, indicating that the martensite starting (Ms) temperatures of the alloys were all below room temperature [36]. Only equiaxed β grains were observed in all the Ti–xNb–0.4O alloys by optical microscopy, as shown in Fig. 1b. The α" phase was hardly observed in Ti–(30, 32, 34)Nb–0.4O alloys primarily owing to the small size. Some lath structures were observed in the TEM bright-field image of Ti–30Nb–0.4O (Fig. 2a). Weak diffraction spots corresponding to the α" phase and ω phase were found in the selected area electron diffraction (SAED) pattern (Fig. 2b). The nano-sized ω phase and lamellar α" phase were observed in the TEM dark field images, respectively (Fig. 2c and d).

For the Ti–Nb binary alloys with Nb content ranging from 30% to 38%, the diffraction peaks corresponding to α" phase and ω phase were found in the XRD patterns, and dense α" phase with acicular structure was usually observed by optical microscopy [3,37–39]. In this study, the α" phase was hardly observed by optical microscopy, and ω phase was not detected by XRD. Small-sized α" phase and ω phase were observed by TEM, indicating that both α" phase and ω phase transformations during quenching were inhibited by O addition.

3.3. Tensile behaviors

The true stress–strain curves and the corresponding work-hardening rate curves of the alloys calculated from the tensile engineering curves are shown in Fig. 3. Obvious yielding between elastic deformation and plastic deformation was hardly observed in the curves of the Ti–(30, 32, 34, 36, 38)Nb–0.4O alloys, owing to the metastable β phase [16,40].

Table 1
Chemical compositions of the Ti–xNb–0.4O alloys (mass%).

Alloys	Ti	Nb	O
Ti-30Nb-0.4O	Bal.	29.8	0.45
Ti-32Nb-0.4O	Bal.	32.3	0.47
Ti-34Nb-0.4O	Bal.	34.1	0.48
Ti-36Nb-0.4O	Bal.	35.1	0.47
Ti-38Nb-0.4O	Bal.	38.5	0.46
Ti-40Nb-0.4O	Bal.	39.4	0.47
Ti-42Nb-0.4O	Bal.	41.9	0.41

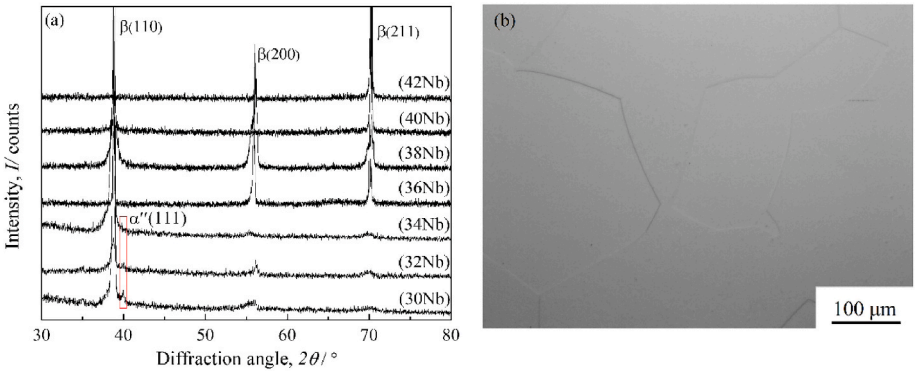

Fig. 1. (a) XRD patterns of the Ti–*x*Nb–0.4O alloys and (b) optical microstructure of Ti–30Nb–0.4O subjected to solution treatment.

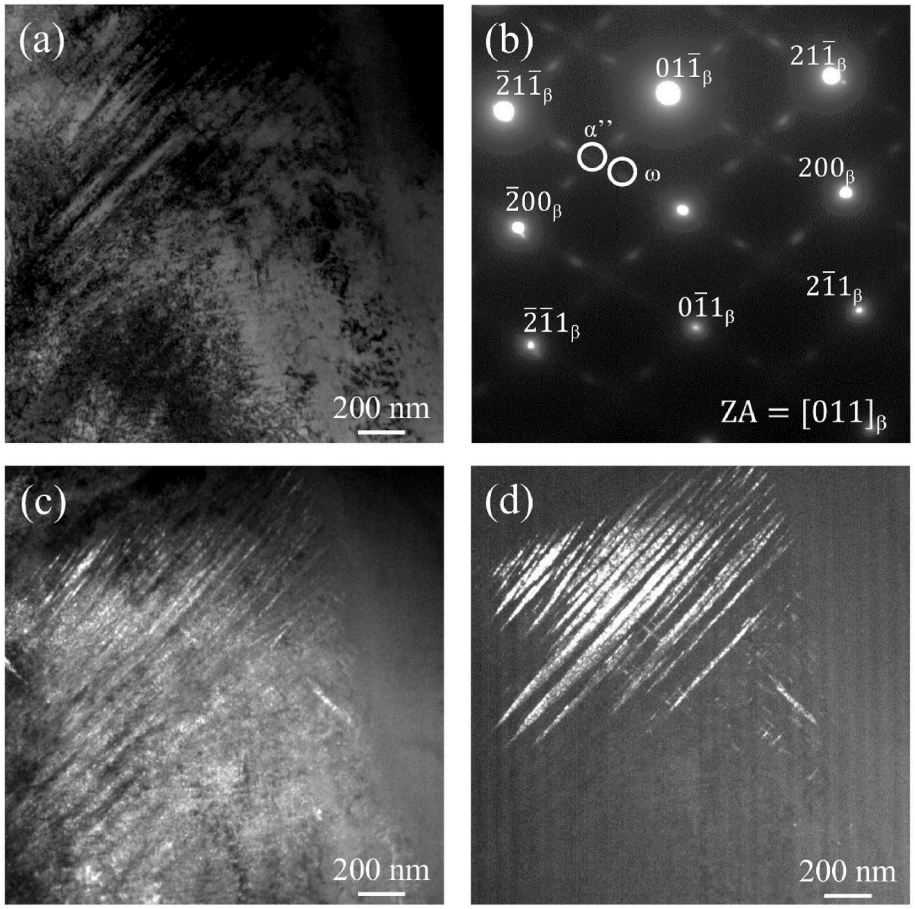

Fig. 2. TEM results of Ti–30Nb–0.4O subjected to solution treatment: (a) bright field image, (b) SAED pattern, (c) dark field image of ω phase, and (d) dark field image of α" phase.

Yielding occurred in Ti–(40, 42)Nb–0.4O, suggesting that the β phase was stable. After elastic deformation, the Ti–(30, 32, 34, 36, 38) Nb–0.4O alloys showed a gradual increase in stress with an increase in strain during the plastic deformation stage, suggesting work-hardening behavior. The stress of Ti–40Nb–0.4O increased slightly from yielding to fracture. Ti–42Nb–0.4O exhibited typical yielding behavior. The stress decreased after elastic deformation and then increased slightly during plastic deformation.

The work-hardening rate (θ) curves of the Ti–(30, 32, 34, 36, 38, 40, 42)Nb–0.4O alloys were calculated from the true stress–strain curves using the following equation:

$$\theta = d\sigma_T/d\varepsilon_T$$

where σ_T is the true stress, ε_T is the true strain, and $d\sigma_T/d\varepsilon_T$ is the work-hardening rate [41].

The work-hardening rate was very high in the elastic deformation of all the Ti–Nb–O alloys because the stress rapidly increased with the increase in strain. The intersection point between the true stress–strain curve and the work-hardening rate curve was marked by a circle in each figure. For the plastic deformation part of the Ti–(30, 32, 34, 36, 38) Nb–0.4O alloys, the work-hardening rate was maintained at a high level with the increase in strain because they had a good work-hardening ability. A sharp decrease in the work-hardening rate occurred near the strain corresponding to the maximum stress. When the strain was further increased from the intersection point, the stress quickly reached the

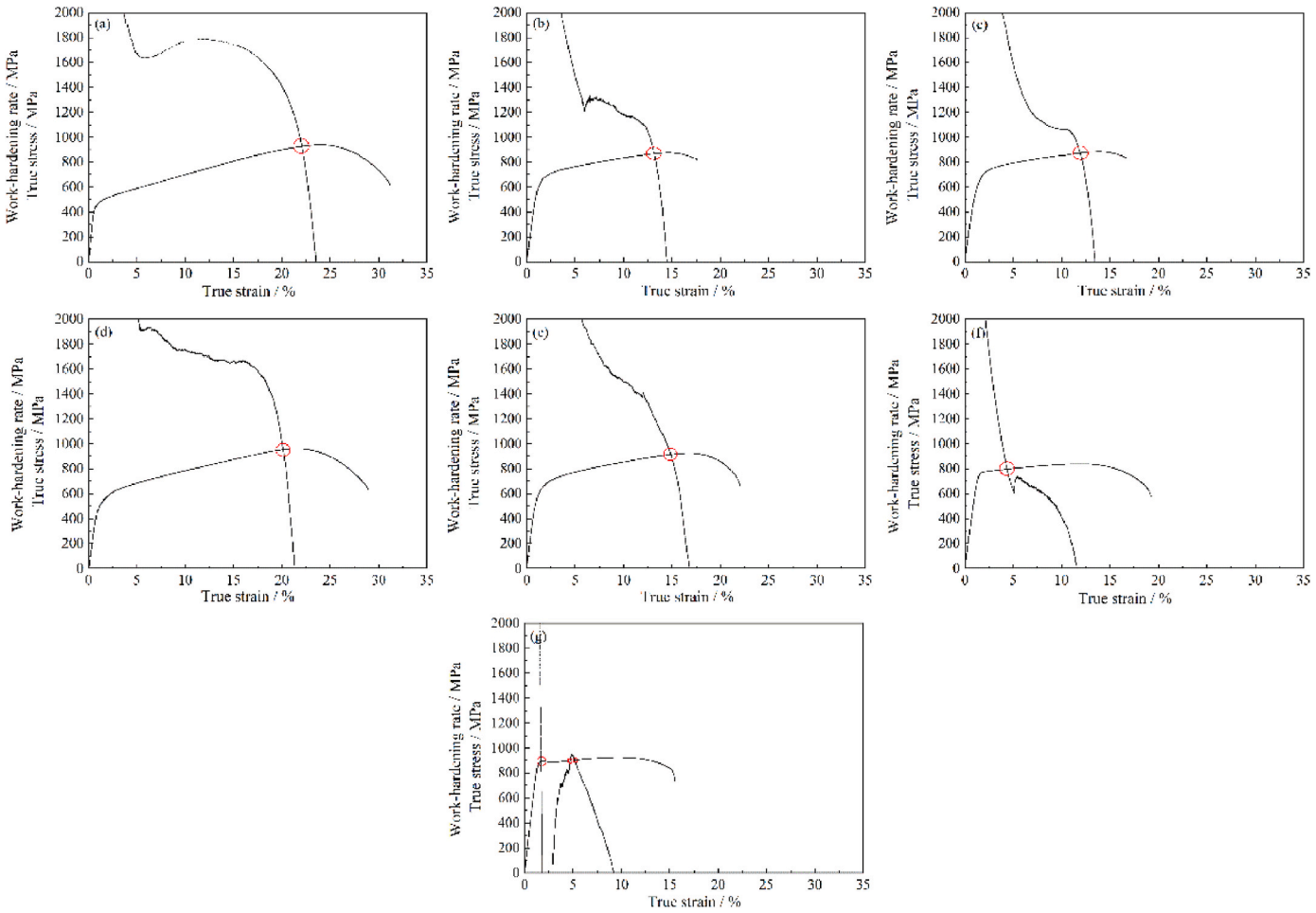

Fig. 3. True stress–strain curves and work-hardening curves of (a) Ti–30Nb–0.4O, (b) Ti–32Nb–0.4O, (c) Ti–34Nb–0.4O, (d) Ti–36Nb–0.4O, (e) Ti–38Nb–0.4O, (f) Ti–40Nb–0.4O, and (g) Ti–42Nb–0.4O.

maximum value, the work-hardening rate decreased to 0, and fracture occurred. As the yield appeared in the Ti–(40, 42)Nb–0.4O alloys, the intersection points were located near the yielding points. For Ti–40Nb–0.4O, the work-hardening rate was maintained at a low level with increasing strain, suggesting a weak work-hardening ability. For Ti–42Nb–0.4O, there were three intersection points. The first intersection point was localized at the strain immediately after the elastic deformation. The work-hardening rate became negative because the stress decreased with increasing strain during yielding. The work-hardening rate then became positive and increased with increasing strain, indicating that work-hardening occurred and became stronger. After intersecting with the stress–strain curve, the work-hardening rate decreased again and intersected with the stress–strain curve. The work-hardening rate curve revealed the deformation process of Ti–42Nb–0.4O, including yielding, plastic deformation with low work-hardening ability, and fracture. Compared to the Ti–(30, 32, 34, 36, 38)Nb–0.4O alloys, the Ti–(40, 42)Nb–0.4O alloys did not show quick fracture after the intersection points, and the work-hardening rates slowly decreased to 0. The tensile behaviors of Ti–(30, 32, 34, 36, 38) Nb–0.4O alloys quite agree with the view that the intersection point is generally regarded as the "necking point" in the tensile process [30]. However, this view is not consistent with the behavior of Ti–(40, 42) Nb–0.4O alloys. In fact, the disappearance of work-hardening in the plastic deformation stage indicates the end of uniform deformation, that is, the beginning of necking. In other words, when the work-hardening rate decreases to 0, the stress reaches the maximum value, and necking begins with a further increase in the strain. For the Ti–(30, 32, 34, 36, 38)Nb–0.4O alloys, the strain corresponding to the work-hardening rate of 0 was very close to the intersection point; therefore, they agreed with the general view. For the Ti–(40, 42) Nb–0.4O alloys, uniform deformation continued for a while under a low work-hardening rate, and necking was postponed.

Many deformation bands were observed in the deformed Ti–30Nb–0.4O alloy, as shown in Fig. 4a. The deformation bands decreased with increasing Nb content (Fig. 4b) and disappeared for Ti–40Nb–0.4O (Fig. 4c). The bands were evident according to the EBSD observations, as shown in Fig. 5a. An approximately 50.5° misorientation between the bands and the matrix was found by measuring the point-to-origin misorientation (Fig. 5b) from point A to point B in Fig. 5a, suggesting that the deformation bands were {332}β<113>β twinning [42,43]. The high work-hardening rate of Ti–(30, 32, 34, 36, 38)Nb–0.4O alloys was primarily attributed to dynamic strengthening caused by twinning [42]. With the increase of Nb content, the decrease of the bands also indicated the increase of β stability.

3.4. Mechanical properties

Because yielding was hardly observed in the Ti–(30, 32, 34, 36, 38) Nb–0.4O alloys, a 0.2% proof stress ($\sigma_{0.2}$) was calculated and denoted as the yield strength (σ_y). For the Ti–(40, 42)Nb–0.4O alloys with obvious yielding, the lowest stress after yielding was selected as the yield strength (σ_y). Fig. 6 shows the Young's modulus (E) measured by the free-resonance method and the yield strength (σ_y), tensile strength (σ_b), and elongation (ε_l) measured by the tensile test. The changes in

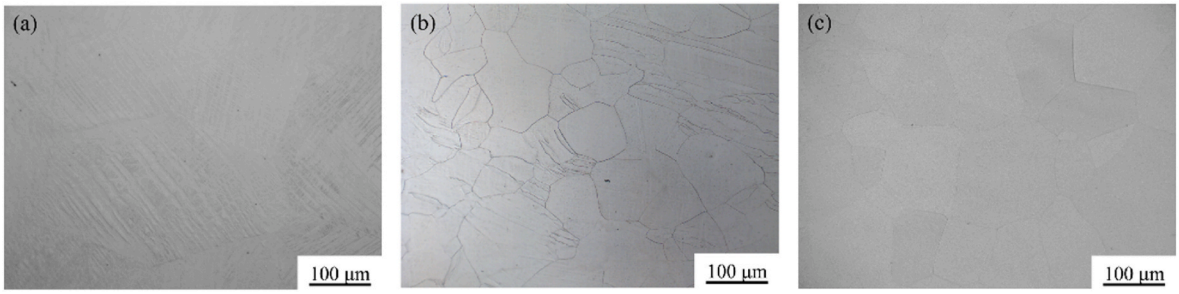

Fig. 4. Optical microstructures of (a) Ti–30Nb–0.4O, (b) Ti–38Nb–0.4O, and (c) Ti–40Nb–0.4O after tensile tests.

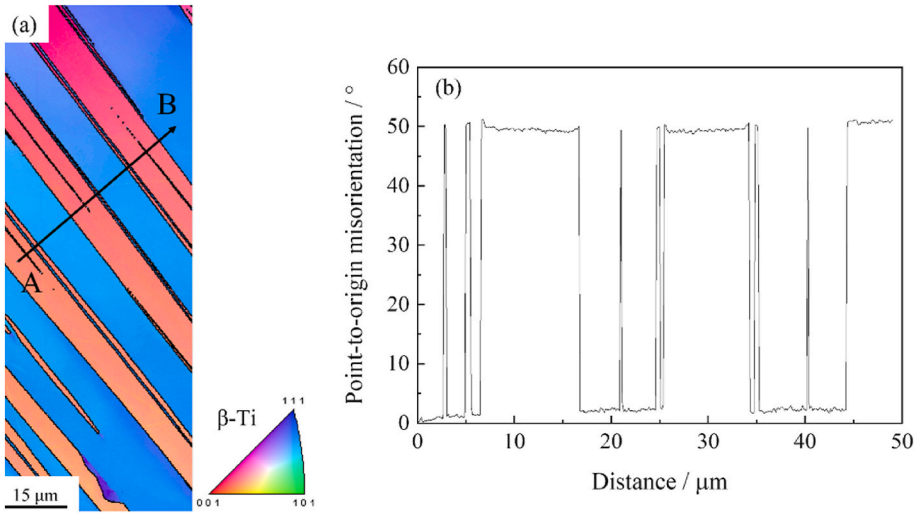

Fig. 5. EBSD results of Ti–38Nb–0.4O after tensile test: (a) EBSD map with IPF color coding and (b) point-to-origin misorientations from A to B in (a).

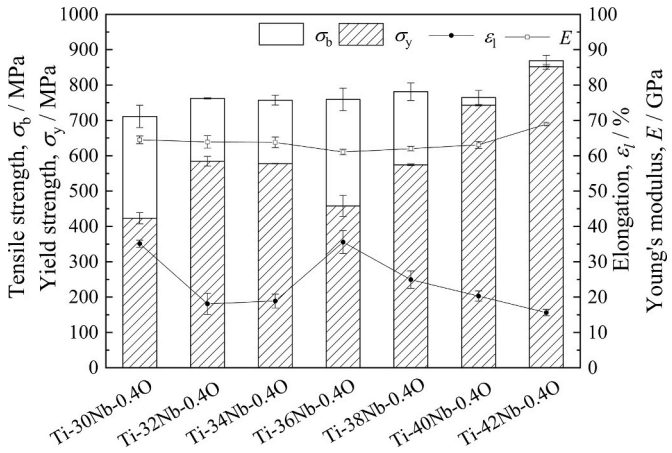

Fig. 6. Mechanical properties of the Ti–*x*Nb–0.4O alloys measured by the free resonance method (*E*) and tensile tests (σ_y, σ_b, and ε_l) at room temperature.

mechanical properties were primarily attributed to the phase compositions and β phase stability. With the increase of the β stabilizer, the α′ phase, α" phase, and ω phase sequentially appear and disappear after solution treatment [44]. A single β phase can be obtained in alloys with sufficient β stabilizer. The Young's modulus of the phase from high to low is $E_\omega > E_{\alpha'} > E_{\alpha''} \approx E_\beta$ [45]. The α" phase is typically soft and ductile, whereas the ω phase is hard and brittle [46]. Ti–30Nb–0.4O consisted of α" phase, ω phase, and β phase and showed a Young's modulus of ~64 GPa, a σ_y of ~423 MPa, and a σ_b of ~711 MPa, respectively. It was reported that the α" phase disappears prior to the ω phase with the increase of β stability [44]. In this study, the α" phase first disappeared with increasing Nb content in the Ti–*x*Nb–0.4O alloys, but the ω phase still existed in Ti–32Nb–0.4O and Ti–34Nb–0.4O. Thus, the *E* was almost constant, the ε_l decreased, and the σ_y increased. When the Nb content was further increased to 36%, the ω phase was also inhibited, so the *E* and σ_y decreased together with ε_l increasing. The lowest Young's modulus is generally obtained for alloys with the β stability shifting from metastable to stable, and a lower σ_y is related to the unstable β lattice [47,48]. It is believed that Ti–36Nb–0.4O is close to the critical component. When the Nb content was increased from 36% to 42%, the β phase was changed from a metastable state to a stable state, and the *E* and σ_y increased with the further increase of β stability. Ti–36Nb–0.4O exhibits the lowest Young's modulus of approximately 61 GPa, whereas Ti–42Nb–0.4O exhibits the highest Young's modulus of approximately 68 GPa. Moreover, the σ_y gradually increased to ~851 MPa for Ti–42Nb–0.4O. The Ti–(32, 34, 36, 38, 40)Nb–0.4O alloys exhibited a similar σ_b of approximately 760 MPa and the σ_b of Ti–42Nb–0.4O was as high as ~869 MPa. Both Ti–32Nb–0.4O and Ti–34Nb–0.4O showed a similar ε_l of ~18%, which is lower than those of Ti–30Nb–0.4O and Ti–36Nb–0.4O. Twinning can supply twinning-induced plasticity in the Ti alloy with a metastable β phase, which is suppressed by excessive β stabilizer addition [49]. When the Nb content increased from 36% to 42%, the ε_l gradually decreased from ~35% to ~16%, primarily because of the disappearance of twinning.

3.5. Discussion

For β-type Ti alloys, the occurrences of the double yielding phenomenon, nonlinear deformation, and {332}β<113>β twinning during the deformation process are all mainly due to the instability of the β

phase, and they disappear in the alloy with stable β phase [49]. For Ti–Nb binary alloys, the α" phase can be found in the solution-treated alloys with Nb content up to 38% (24 mol.%), the ω phase can be found in the solution-treated alloys with Nb content up to 40.5% (26 mol.%), and double yielding phenomenon still appears in Ti–42Nb (Ti–27Nb in mol.%) [50,51]. O can effectively decrease the Ms temperatures of Ti alloys [52]. In this study, the double-yielding phenomenon did not appear in the studied Ti–Nb–O alloys, indicating that stress-induced martensite transformation (SIMT) did not occur. However, twinning occurred in the Ti–Nb–O alloys, with the Nb content up to 38%. It suggests that O effectively suppresses the ω phase and α" phase transformations during quenching and SIMT during tension but does not strongly suppress deformation twinning. Therefore, the metastable β phase can be maintained in Ti–*x*Nb–0.4O alloys with a large range of Nb content, which is beneficial for obtaining a low Young's modulus.

O also showed effective solution strengthening in the Ti–*x*Nb–0.4O alloys. The Ti–(36, 38, 40)Nb–0.4O alloys with the Young's moduli of 61–63 GPa showed a relatively high σ_b up to 760 MPa, which was much higher than previously reported low-modulus β-type Ti alloys, such as Ti–29Nb–13Ta–4.6Zr and Ti–35Nb–7Zr–5Ta [49,53,54]. For the alloy with a stable β phase, the σ_b is often lower than that of the alloy with the metastable β phase owing to the disappearance of dynamic reinforcement caused by twinning [34,48]. In this study, Ti–42Nb–0.4O showed a σ_b of up to ~869 MPa, which was close to that of some α+β-type Ti alloys, such as Ti–6Al–4V ELI (~895 MPa) and Ti–13Nb–13Zr (~996 MPa), and its Young's modulus was lower than those of the alloys [55,56]. The Ti–(36, 38, 40, 42)Nb–0.4O alloys exhibited different yield ratios. It is supposed that Ti–36Nb–0.4O, with a lower yield ratio, is easily formed by cold deformation. By contrast, the Ti–(40, 42)Nb–0.4O alloys with a higher σ_y and a higher yield ratio have a higher ability to resist plastic deformation. Therefore, the present studied Ti–(36, 38, 40, 42)Nb–0.4O can satisfy different requirements of mechanical properties for applications. In particular, Ti–36Nb–0.4O shows good comprehensive mechanical properties, including a low Young's modulus, high strength, and good plasticity, and is suitable for hard-tissue replacement.

4. Conclusions

The following conclusions can be drawn from the above results and discussion:

(1) O content of 0.4–0.5% in Ti–Nb alloys was obtained by adding 0.3% O to the alloys in the form of TiO_2. The formations of the α" phase and ω phase during quenching are suppressed by O addition.
(2) The metastable β phase deforming behavior, including twinning are found in the Ti–(30, 32, 34, 36, 38)Nb–0.4O alloys, and the Ti–(40, 42)Nb–0.4O alloys show a stable β phase deforming behavior. The solution strengthening of O results in high tensile strength, regardless of twinning deformation.
(3) The 0.4% O added Ti–Nb alloys exhibited desirable mechanical properties, including high strength, low Young's modulus, and good plasticity.

CRediT authorship contribution statement

Qiang Li: Writing – review & editing, Writing – original draft, Investigation. **Yan Liu:** Writing – review & editing, Writing – original draft, Investigation. **Huanhuan Yu:** Investigation. **Masaaki Nakai:** Investigation. **Mitsuo Niinomi:** Investigation. **Kenta Yamanaka:** Investigation. **Akihiko Chiba:** Investigation. **Takuya Ishimoto:** Investigation. **Takayoshi Nakano:** Investigation.

Declaration of competing interest

The authors declare that they have no known competing financial interests or personal relationships that could have appeared to influence the work reported in this paper.

Data availability

Data will be made available on request.

Acknowledgements

This work was partially supported by the Shanghai Engineering Research Center of High-Performance Medical Device Materials (No. 20DZ2255500), and the Grant-in Aid for Scientific Research (C) (No. 20K05139) from JSPS (Japan Society for the Promotion of Science), Tokyo, Japan.

References

[1] M. Gepreel, M. Niinomi, Biocompatibility of Ti-alloys for long-term implantation [J], J. Mech. Behav. Biomed. Mater. 20 (2013) 407–415.
[2] D. Banerjee, J.C. Williams, Perspectives on titanium science and technology [J], Acta Mater. 61 (3) (2013) 844–879.
[3] M. Bonisch, M. Calin, J. Humbeeck, et al., Factors influencing the elastic moduli, reversible strains and hysteresis loops in martensitic Ti-Nb alloys [J], Mater. Sci. Eng. C 48 (2015) 511–520.
[4] Z. Ren, W. Liu, Q. An, et al., Microstructures and tensile properties of low-cost TiBw/Ti–6Al–4V composites by vacuum reactive hot pressing [J], Vacuum (2023) 211, 111921.
[5] M. Long, H.J. Rack, Titanium alloys in total joint replacement—a materials science perspective [J], Biomaterials 19 (1998) 1621–1639.
[6] Y. Okazaki, S. Rao, Y. Ito, et al., Corrosion resistance, mechanical properties, corrosion fatigue strength and cytocompatibility of new Ti alloys without Al and V [J], Biomaterials 19 (1998) 1197–1215.
[7] Y. Zhou, M. Niinomi, T. Akahori, et al., Corrosion resistance and biocompatibility of Ti–Ta alloys for biomedical applications [J], Mater. Sci. Eng. A 398 (1–2) (2005) 28–36.
[8] L. Zhou, J. Sun, X. Bi, et al., Effect of scanning strategies on the microstructure and mechanical properties of Ti–15Mo alloy fabricated by selective laser melting [J], Vacuum 205 (2022), 111454.
[9] J. Xu, S. Tao, L. Bao, et al., Effects of Mo contents on the microstructure, properties and cytocompatibility of the microwave sintered porous Ti-Mo alloys [J], Mater. Sci. Eng. C 97 (2019) 156–165.
[10] Y. Zhou, M. Niinomi, T. Akahori, Effects of Ta content on Young's modulus and tensile properties of binary Ti–Ta alloys for biomedical applications [J], Mater. Sci. Eng. A 371 (1–2) (2004) 283–290.
[11] D. Zhang, J.G. Lin, W. Jiang, et al., Shape memory and superelastic behavior of Ti–7.5Nb–4Mo–1Sn alloy [J], Mater. Des. 32 (8–9) (2011) 4614–4617.
[12] W. Ho, C. Ju, L. Chern, Structure and properties of cast binary Ti–Mo alloys, J]. Biomaterials (20) (1999) 2115–2122.
[13] D. Zhang, Y. Mao, Y. Li, et al., Effect of ternary alloying elements on microstructure and superelastictity of Ti–Nb alloys [J], Mater. Sci. Eng. A 559 (2013) 706–710.
[14] S. Zhang, J. Zhang, S. Ma, et al., Microstructure and mechanical properties of Ta–Ti alloy by plasma-activated sintering [J], Vacuum 206 (2022), 111554.
[15] M. Geetha, A. Singh, R. Asokamani, et al., Ti based biomaterials, the ultimate choice for orthopaedic implants – a review [J], Prog. Mater. Sci. 54 (3) (2009) 397–425.
[16] J. Wang, W. Xiao, L. Ren, et al., The roles of oxygen content on microstructural transformation, mechanical properties and corrosion resistance of Ti-Nb-based biomedical alloys with different β stabilities [J], Mater. Char. 176 (2021), 111122.
[17] H.Y. Kim, H. Satoru, J.I. Kim, et al., Mechanical properties and shape memory behavior of Ti-Nb alloys [J], Mater. Trans. 45 (7) (2004) 2443–2448.
[18] T. Ozaki, H. Matsumoto, S. Watanabe, et al., Beta Ti alloys with low Young's modulus [J], Mater. Trans. 45 (8) (2004) 2776–2779.
[19] Q. Li, M. Niinomi, M. Nakai, et al., Effect of Zr on super-elasticity and mechanical properties of Ti–24at% Nb–(0, 2, 4)at% Zr alloy subjected to aging treatment [J], Mater. Sci. Eng. A 536 (2012) 197–206.
[20] Q. Li, T. Liu, J. Li, et al., Microstructure, mechanical properties, and cytotoxicity of low Young's modulus Ti–Nb–Fe–Sn alloys [J], J. Mater. Sci. 57 (9) (2022) 5634–5644.
[21] S. Gu, Z. Zhou, N. Min, Effects of element (Al, Mo, Sn and Fe) doping on phase structure and mechanical properties of the Ti-Nb-based alloys, [J]. Metals 12 (8) (2022) 1249.
[22] M. Wasz, F. Brotzen, R. Mclellan, et al., Effect of oxygen and hydrogen on mechanical properties of commercial purity titanium [J], Int. Mater. Rev. 41 (1) (1996) 1–12.
[23] R. Salloom, D. Reith, R. Banerjee, et al., First principles calculations on the effect of interstitial oxygen on phase stability and β–α'' martensitic transformation in Ti–Nb alloys [J], J. Mater. Sci. 53 (16) (2018) 11473–11487.
[24] C. Liu, L. Yu, Y. Liu, et al., Interactions between interstitial oxygen and substitutional niobium atoms in Ti–Nb–O BCC alloys: first-principles calculations [J], AIP Adv. 10 (2) (2020), 025309.

[25] M. Tane, T. Nakano, S. Kuramoto, et al., ω Transformation in cold-worked Ti–Nb–Ta–Zr–O alloys with low body-centered cubic phase stability and its correlation with their elastic properties [J], Acta Mater. 61 (1) (2013) 139–150.
[26] E. Lopes, L. Santos, R. Caram, et al., Achieving high strength and low Young's modulus in martensitic Ti-Nb-O alloys [J], Mater. Lett. 301 (2021), 130308.
[27] S. BartáKOVá, J. MáLEK, P. PrachâR, The effect of oxygen addition on microstructure and mechanical properties of various beta-titanium alloys [J], JOM 72 (4) (2019) 1656–1663.
[28] M. Yan, W. Xu, M.S. Dargusch, et al., Review of effect of oxygen on room temperature ductility of titanium and titanium alloys [J], Powder Metall. 57 (4) (2014) 251–257.
[29] Q. Yu, L. Qi, T. Tsuru, et al., Origin of dramatic oxygen solute strengthening effect in titanium [J], Materials and Methods 347 (6222) (2015) 635–639.
[30] H. Liu, M. Niinomi, M. Nakai, et al., Abnormal deformation behavior of oxygen-modified β-type Ti-29Nb-13Ta-4.6Zr alloys for biomedical applications [J], Metall. Mater. Trans. A 48 (1) (2016) 139–149.
[31] F. Geng, M. Niinomi, M. Nakai, Observation of yielding and strain hardening in a titanium alloy having high oxygen content [J], Mater. Sci. Eng. 528 (16–17) (2011) 5435–5445.
[32] P. Laheurte, F. Prima, A. Eberhardt, et al., Mechanical properties of low modulus beta titanium alloys designed from the electronic approach [J], J. Mech. Behav. Biomed. Mater. 3 (8) (2010) 565–573.
[33] Q. Li, D. Ma, J. Li, et al., Low Young's modulus Ti–Nb–O with high strength and good plasticity [J], Mater. Trans. 59 (5) (2018) 858–860.
[34] Y. Hon, J. Wang, Y. Pan, Composition phase structure and properties of titanium-niobium alloys [J], Mater. Trans. 44 (11) (2003) 2384–2390.
[35] Y.L. Hao, M. Ninomi, D. Kuroda, et al., Young's modulus and mechanical properties of Ti-29Nb-13Ta-4.6Zr in relation to α'' martensite [J], Metall. Mater. Trans. A 33 (2002) 3137–3144.
[36] M. Tahara, T. Inamura, H.Y. Kim, et al., Role of oxygen atoms in α'' martensite of Ti-20 at.% Nb alloy [J], Scripta Mater. 112 (2016) 15–18.
[37] E. Hildyard, L. Connor, L. Owen, et al., The influence of microstructural condition on the phase transformations in Ti-24Nb (at.%) [J], Acta Mater. 199 (2020) 129–140.
[38] L. Chang, Y. Wang, Y. Ren, In-situ investigation of stress-induced martensitic transformation in Ti–Nb binary alloys with low Young's modulus [J], Mater. Sci. Eng. A 651 (2016) 442–448.
[39] C.Y. Cui, D.H. Ping, Microstructural evolution and ductility improvement of a Ti–30Nb alloy with Pd addition [J], J. Alloys Compd. 471 (1–2) (2009) 248–252.
[40] F.Q. Hou, S.J. Li, Y.L. Hao, et al., Nonlinear elastic deformation behaviour of Ti–30Nb–12Zr alloys [J], Scripta Mater. 63 (1) (2010) 54–57.
[41] J.D. Embury, W.J. Poole, D.J. Lloyd, The work hardening of single phase and multi-phase aluminium alloys [J], Mater. Sci. Forum 519–521 (2006) 71–78.
[42] Y. Im, Y. Lee, Effects of Mo concentration on recrystallization texture, deformation mechanism and mechanical properties of Ti–Mo binary alloys [J], J. Alloys Compd. 821 (2020), 153508.
[43] E. Bertrand, P. Castany, I. PéRON, et al., Twinning system selection in a metastable β-titanium alloy by Schmid factor analysis [J], Scripta Mater. 64 (12) (2011) 1110–1113.
[44] Y. Hao, S. Li, S. Sun, et al., Elastic deformation behaviour of Ti-24Nb-4Zr-7.9Sn for biomedical applications [J], Acta Biomater. 3 (2) (2007) 277–286.
[45] A. Panigrahi, M. BöNISCH, T. Waitz, et al., Phase transformations and mechanical properties of biocompatible Ti–16.1Nb processed by severe plastic deformation [J], J. Alloys Compd. 628 (2015) 434–441.
[46] P. Żywicki, D. Ping, T. Abe, et al., Effect of Pd addition on the microstructure of Ti-30Nb alloy [J], Met. Mater. Int. 21 (4) (2015) 617–622.
[47] W. Kim, H. Kim, Effect of oxygen on elastic modulus and mechanical property of metastable β TiNbO based alloys [J], Key Eng. Mater. 342–343 (2007) 549–552.
[48] R.P. Kolli, W.J. Joost, S. Ankem, Phase stability and stress-induced transformations in beta titanium alloys [J], Jom 67 (6) (2015) 1273–1280.
[49] Q. Li, Q. Qi, J. Li, et al., Low springback and low Young's modulus in Ti–29Nb–13Ta–4.6Zr alloy modified by Mo addition [J], Mater. Trans. 60 (9) (2019) 1755–1762.
[50] H. Kim, J. Kim, T. Inamura, et al., Effect of thermo-mechanical treatment on mechanical properties and shape memory behavior of Ti–(26–28) at.% Nb alloys [J], Mater. Sci. Eng. A 438–440 (2006) 839–843.
[51] S. Guo, J. Zhang, X. Cheng, et al., A metastable β-type Ti–Nb binary alloy with low modulus and high strength [J], J. Alloys Compd. 644 (2015) 411–415.
[52] J. Kim, H.Y. Kim, H. Hosoda, et al., Shape memory behavior of Ti-22Nb-(0.5-2.0)O (at%) biomedical alloys [J], Mater. Trans. 46 (4) (2005) 852–857.
[53] J.I. Qazi, H.J. Rack, Metastable beta titanium alloys for orthopedic applications [J], Adv. Eng. Mater. 7 (11) (2005) 993–998.
[54] T. Lee, M. Nakai, M. Niinomi, et al., Phase transformation and its effect on mechanical characteristics in warm-deformed Ti-29Nb-13Ta-4.6Zr alloy [J], Met. Mater. Int. 21 (1) (2015) 202–207.
[55] L. Zhou, T. Yuan, R. Li, et al., Anisotropic mechanical behavior of biomedical Ti-13Nb-13Zr alloy manufactured by selective laser melting [J], J. Alloys Compd. 762 (2018) 289–300.
[56] L.C. Zhang, L.Y. Chen, A review on biomedical titanium alloys: recent progress and prospect [J], Adv. Eng. Mater. 21 (4) (2019), 1801215.